INSTITUTE OF PHYSICS PUBLISHING JOURNAL OF PHYSICS D: APPLIED PHYSICS

J. Phys. D: Appl. Phys. **39** (2006) 3665–3673 doi:10.1088/0022-3727/39/16/021

Deformation of elastic coatings in adhesive contacts with spherical probes

P Mary, A Chateauminois[1] and C Fretigny

Laboratoire de Physico-Chimie des Polymères et des Milieux Dispersés, UMR CNRS 7615 Ecole de Physique et Chimie Industrielles (ESPCI), 10 rue Vauquelin, 75213 Paris Cedex 05, France

E-mail: antoine.chateauminois@espci.fr

Received 9 May 2006, in final form 26 June 2006
Published 4 August 2006
Online at stacks.iop.org/JPhysD/39/3665

Abstract

This study addresses the problem of adhesive contacts between layered substrates and axisymmetric probes. A semi-analytical approach to adhesive contacts has been developed as an extension of a model recently published by Perriot and Barthel (2004 *J. Mat. Res.* **19** 600–8) for the axisymmetric elastic indentation of non-adhesive, coated substrates. In addition to the load and penetration at equilibrium, the model allowed the derivation of the shape of the free surface in the contact zone. The validity of the approach was verified from experiments using contacts between acrylate films above their glass transition temperature (T_g) and spherical glass lenses. When the adhesive contacts were quenched below T_g, stable imprints were obtained which allowed determination of the surface deformations of the films. The latter were found consistent with the hypothesis of short range surface forces which were embedded in the contact model. Deviations from theory in the form of fingering instabilities at the periphery of the contact were observed when the confinement of the film was increased. A calculation of the stresses within the adhesive contacts indicated that these instabilities are probably driven by the release of lateral constraints within the confined films.

1. Introduction

Adhesive forces acting within contacts between thin compliant layered surfaces are an important aspect in the mechanical and tribological behaviour of many devices. Soft bearing surfaces in artificial joint replacements or microelectromechanical systems, pressure sensitive adhesives or experiments using microprobe instruments such as the surface force apparatus and the atomic force microscope are a few examples where the response of the system is strongly affected by adhesion.

A major development in the contact mechanics of soft adhesive surfaces is the Johnson–Kendall–Roberts (JKR) theory which extends the Hertzian analysis to contacts under the action of short range atomic forces [1]. This theory has been shown to be valid in situations where the action of the adhesive forces can be neglected outside the contact, which was found to be a valid assumption for soft materials such as elastomers [2,3]. Accordingly, a commonly called JKR test was developed which consists in compressing a soft elastic sphere against a flat rigid surface or, conversely, a hard sphere against a flat soft elastic medium. This test emerged as a convenient method to determine the work of adhesion between materials from a measurement of the relationship between the contact area and the applied force within macroscopic contacts (see, for example, [4, 5]). In addition, the JKR theory has also been used as a basis to analyse more recent adhesion experiments carried out at the submicrometric scale using AFM [6] or nano-indentation [7, 8].

However, the JKR model was developed within the assumption that the size of the contact remains small compared with the dimensions of the contacting bodies and some problems arise when it is applied to thin films. As the ratio of the contact radius to the film thickness is increased, substrate effects come into play which induce a deviation from the JKR theory. Similar finite size effects were also reported during JKR experiments when small elastomers lens were used [9].

[1] Author to whom any correspondence should be addressed.

Schull [10] reviewed current approaches to this finite size problem within the context of the adhesion of compliant incompressible films perfectly bounded to rigid substrates. As in the classical JKR theory, the adhesion of thin films can be treated from a thermodynamical standpoint, which relies on a determination of the elastic energy stored within the contact. This latter calculation requires making use of the compliance of the non-adhesive coated contact. In the absence of any tractable analytical solution to this contact mechanics problem, it was initially proposed by Shull and coworkers to derive empirical closed-form expressions for the contact compliance from finite element (FE) simulations [11, 12]. More recently, similar FE approaches to coated adhesive contacts have been extended by Shridhar and Johnson [13–16] to the case of elastic substrates considering both compressible and incompressible coatings. These calculations especially showed that some of the adhesion characteristics such as the pull-off force can be influenced by the elastic properties of the contacting solids, which is not the case for homogeneous contacts.

In the present study, an alternative analytical approach to the mechanics of adhesive contacts between coated substrates and rigid axisymmetric probes is developed as an extension of a model recently developed by Perriot and Barthel [17] for the non-adhesive case. The approach is developed within the framework of the JKR assumption that surface forces do not act outside the contact. From a determination of the elastic energy stored within the system, we show that the adhesion energy can very easily be incorporated within the theory in order to provide a semi-analytical description of the adhesive contact at equilibrium. This model is subsequently used to analyse adhesion experiments between acrylate coatings and spherical glass probes. In addition to the description of usual contact parameters such as load and size, an original procedure using the glass transition properties of the coating allowed us to investigate the shape of the adhesive contacts. The observation of a vertical junction of the surface of the film to the rigid spherical indentor especially provided some direct confirmation of the validity of the JKR assumption for the investigated system. When the confinement of the film was increased, some deviations from the theory were, however, observed in the form of periodic instabilities at the periphery of the contact.

2. Experimental details

A specific procedure was developed in order to obtain, at room temperature, a stable imprint of the adhesive contact formed at high temperature between a rubbery polymer and a spherical probe. This methodology was based upon the changes in the mechanical properties of polymers through their glass transition zone. As detailed in figure 1, the test procedure involved three successive stages. In a first stage, a plano-convex glass lens is deposited at room temperature on the surface of a glassy polymer film well below its glass transition temperature, T_g. Under such conditions, the modulus of the polymer is in the gigapascal range and no significant adhesion occurs between the film and the lens. This system is subsequently heated in an oven well above the glass transition. As a consequence, the modulus of the polymer decreases in the megapascal range, thus allowing an increase in the contact area

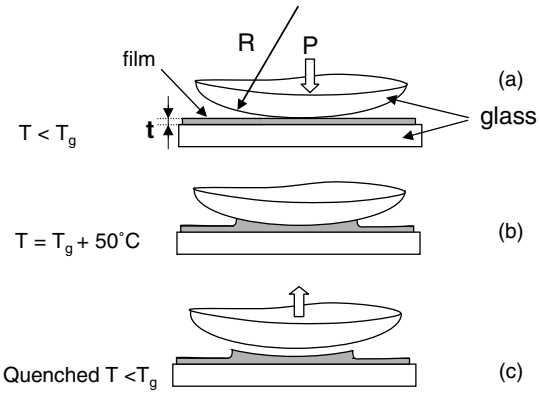

Figure 1. Schematic description of the experimental procedure used for the realization of imprints of adhesive contacts between spherical glass lenses and acrylate films. (*a*) the lens rests on the surface of the glassy film (modulus ∼ GPa), an elastic contact is formed; (*b*) the contact is heated up above T_g, adhesion occurs between the lens and the rubbery coating (modulus ∼ MPa); (*c*) the adhesive contact is frozen in by cooling below T_g, the lens removed in order to reveal the imprint of the adhesive contact.

under the action of adhesive forces. The system is maintained under high temperature for a long time in order to achieve an equilibrium state. The last stage consisted in cooling down the adhesive contact at room temperature, i.e. below T_g. During this cooling step, it was anticipated that any change in the contact size should be slow enough to allow for a quench of the adhesive contact below T_g. After removal of the glass probe, it was therefore possible to analyse the 'frozen' shape of the adhesive contact.

2.1. Materials

The experimental procedure required a polymer with a glass transition above room temperature but not too elevated in order to avoid thermal degradation of the specimens during the development of the adhesive contact. These conditions were fulfilled using a crosslinked acrylate polymer which was obtained from the copolymerization of *n*-butylmethacrylate (Acros Organics, purity 99%) and isobutylmethacrylate (Acros Organics, purity 99%) in a 1.2 : 1.0 molar ratio. The crosslinking agent was butanedioldiacrylate (Lancaster, 85%) with a concentration of 4 mol L^{-1}. Irgacure® 819 (Ciba Specialty Chemicals) was used as an initiator for the radical polymerization of the mixture under the action of UV light.

The adhesive contacts experiments were first validated using bulk specimens 10 mm in thickness. They were polymerized from the monomer mixture between two float glass plates which were treated with dichloromethylsilane as a release agent. The reacting species were exposed to UV light for nine hours. In order to ensure a homogeneous polymerization through the thickness of the specimens, the mould was continuously rotated under the UV lamp. After removing the glass plates, additional heat treatment at 120 °C under vacuum was carried out for 12 h in order to increase the extent of reaction and to eliminate residual unreacted monomers. The glass transition temperature of the resulting polymer was 53 °C, as measured by DSC at 10 °C min^{-1}. This value remained unaffected when DSC specimens were taken

from different locations though the thickness of the acrylate plate, which indicates a good homogeneity of the sample. The polymer gel fraction was found to be greater than 99% after swelling in chloroform and subsequent drying of specimens. The specimens were stored in a desiccator prior to use.

The films were realized using a similar procedure [18]. The specified film thicknesses (i.e. 15, 33, 80 and 110 μm) were obtained using PET spacers which were inserted between the two glass plates. Prior to polymerization, one of the glass plates was treated with dichloromethylsilane as a release agent; the other one was exposed under nitrogen to a 1% solution of 3-methacryloxy-propyl-dimethyl chlorosilane in toluene in order to promote a chemical bonding between the glass substrate and the polymer film during polymerization. After polymerization, the glass transition of the film was found to be 52 °C by means of DSC at 10 °C min^{-1}. The gel fraction of the film was greater than 90%.

2.2. Contact experiments

Commercially available (Melles Griott, France) boro-silicate glass lenses were used for the contact experiments. The radii of curvature of the selected lenses varied between 3.1 and 77.8 mm and their weights between 0.038 and 2.62 g. From interferometry measurement, the rms roughness of the lenses was found to be of the order of 10 nm for a 500 × 500 μm^2 surface. Prior to use, the lenses were cleaned in a 70 : 30 H_20_2/H_2SO_4 solution and rinsed with distilled water.

Adhesive contacts were formed in a vacuum oven at 100 °C (i.e. about 50 °C above the glass transition temperature) for one night in order to achieve equilibrium. A previously reported dynamic viscoelastic analysis of the used crosslinked acrylate [18] showed that, at this temperature, its low frequency response is essentially of elastic nature with only a very limited viscous dissipation at a scale of 10 s. Moreover, the selected long equilibrium time can be assumed to allow for the relaxation of any residual viscoelastic effects within the adhesive layer.

The contact system was subsequently cooled down to R.T. by opening the door of the oven. Once the contacts were fully vitrified, the lenses were easily removed with no detectable pull-off force. An assessment of the thermal contraction of the film and of the glass sphere during cooling showed that these effects should not modify by more than 1% the actual shape of the adhesive contact. The adhesive imprints were analysed using a non-contact optical profilometer (MicroXAM, Scientec, France) with a height resolution in the nanometre range.

3. Adhesive contact model

3.1. Solution for the adhesive contact problem

Let us consider the system depicted in figure 2, which consists of an elastic substrate coated by an adhesive film in contact with a rigid sphere. E_i and ν_i denote the Young's modulus and the Poisson's ratio of the layer ($i = 1$) and of the substrate ($i = 0$). An analytical model of the adhesive contact between the compliant film and a spherical probe was derived as an extension of an approach to the elastic indentation of coated substrates by rigid indenters which was recently developed by

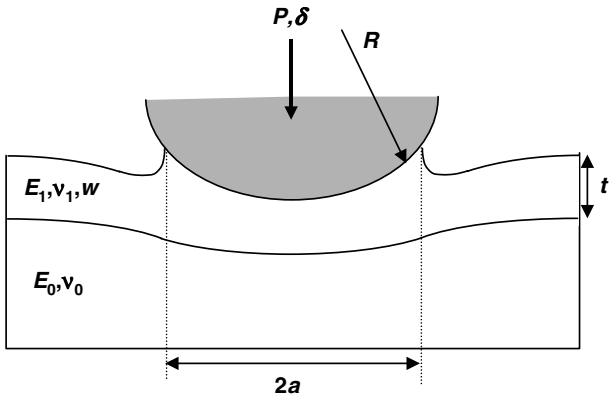

Figure 2. Schematic description of the contact configuration considered for the adhesion model. A rigid sphere of radius, R, contacts an adhesive film of thickness, t, on an elastic substrate. E_i and ν_i are, respectively, the Young's moduli and the Poisson's ratios of the substrate ($i = 0$) and the layer ($i = 1$).

Perriot and Barthel [17]. The model is based on the expression derived independently by Li and Chou [19] and by Nogi and Kato [20] for the Green function for a layered substrate. Within the framework of linear elasticity, these authors have derived an expression relating the Hankel transforms of the normal displacement, $u(r)$, to that of the applied normal stress, $\sigma(r)$, at the surface of the elastic layer:

$$\bar{u}(\xi) = \frac{2}{E_1^*}\frac{X(\xi)}{\xi}\bar{\sigma}(\xi), \tag{1}$$

E_1^* being the reduced modulus of the layer defined as $E_1/(1-\nu_1^2)$where E_1 is the Young's modulus of the coating. $X(\xi)$ is defined as

$$X(\xi) = \frac{1 + 4b\xi t e^{-2\xi t} - abe^{-4\xi t}}{1 - (a + b + 4b(\xi t)^2)e^{-2\xi t} + abe^{-4\xi t}}, \tag{2}$$

$$a = \frac{\alpha\gamma_0 - \gamma_1}{1 + \alpha\gamma_0}, \qquad b = \frac{\alpha - 1}{\alpha + \gamma_1}, \qquad \alpha = \frac{G_1}{G_0},$$
$$\gamma_1 = 3 - 4\nu_1, \qquad \gamma_0 = 3 - 4\nu_0,$$

where G_0 and G_1 denote the shear moduli of the substrate and the layer, respectively and t is the thickness of the coating. In equation (1) , the quantities in the form of $\bar{q}(\xi)$ correspond to the 0th-order Hankel transform of the function $q(r)$ defined as

$$\bar{q}(\xi) = \int_0^\infty \mathrm{d}r\, r J_0(\xi r) q(r)$$

with $J_0(x)$ the 0th-order Bessel function of the first kind.

Due to mixed boundary conditions, the Green function of the coated substrate (equation (1)) cannot be used to provide directly a solution in the real space. However, the use of auxiliary functions developed in [21,22] was shown by Perriot and Barthel [17] to allow the inversion of the contact problem at low numerical cost. Two auxiliary fields, g and θ, were introduced, which correspond to the cosine Fourier transforms of the Hankel transforms of the normal surface stress, $\sigma(r)$,

and displacement, $u(r)$, respectively.

$$g(s) = \int_0^\infty \mathrm{d}\xi \bar{\sigma}(\xi)\cos(\xi s), \tag{3}$$

$$\theta(s) = \int_0^\infty \mathrm{d}\xi \xi \bar{u}(\xi)\cos(\xi s). \tag{4}$$

Alternatively, $\theta(s)$ can also be expressed as

$$\theta(s) = \delta - \varphi(s), \qquad s \leqslant a,$$

where δ is the penetration and $\varphi(s)$ a known function of the geometry of the axisymmetric indenter. In the case of a spherical probe, it can be shown that $\varphi(s) = s^2/R$.

By making use of equations (1), (3) and (4), Perriot and Barthel were able to derive the following integral equation relating, within the contact area (i.e. $s \leqslant a$), the known $\theta(s)$ function to the unknown $g(s)$ function

$$\theta(s) = \frac{2}{E_1^*} g(s) + \int_0^a K(\rho, s) g(\rho)\mathrm{d}\rho, \tag{5}$$

where $K(\rho, s)$ is a symmetric Kernel ($K(\rho, s) = K(s, \rho)$) obtained from a cosine transform of $X(x) = \frac{2}{E_1^*}(C(x) + 1)$.

$$K(\rho, s) = \frac{4}{\pi E_1^*} \int_0^\infty X(\xi t)\cos(\xi s)\cos(\xi\rho)\mathrm{d}\xi, \tag{6}$$

which can be evaluated through simple cosine transform.

The unknown penetration, δ, can easily be eliminated from the problem by writing the integral equation (5) for $s = a$ as

$$\delta - \varphi(a) = \frac{2}{E_1^*} g(a) + \int_0^a K(\rho, a) g(\rho)\mathrm{d}\rho, \tag{7}$$

which after subtraction from equation (5) gives

$$\varphi(a) - \varphi(s) + \frac{2}{E_1^*} g(a) = \frac{2}{E_1^*} g(s) + \int_0^a \Delta K(\rho, a) g(\rho)\mathrm{d}\rho, \tag{8}$$

where $\Delta K(\rho, s) = K(\rho, s) - K(\rho, a)$.

The above integral expression provides the basis for the determination of the normal surface stress beneath the indenter. As compared with the solution developed in [17], this expression incorporates two new features. First, the unknown penetration, δ, has been removed from the integral equation giving $g(s)$, i.e. the normal stress distribution within the contact. Secondly, the solution given by equation (8) takes into account explicitly the value of $g(s)$ for $s = a$, which was implicitly discarded from the solution provided by Perriot and Barthel (i.e. $g(a) = 0$).

It can easily be recognized that the assumption that $g(s)$, i.e. the contact stress, vanishes at the edge of the contact corresponds to non-adhesive contact situations. This description is similar to that introduced by Barquins and Maugis [23] to extend Sneddon analysis of contact mechanics to adhesive situations. However, the model can be extended to equilibrium adhesive contacts if the relationship between $g(a)$ and the reversible work of adhesion is accounted for from a calculation of the energy release rate. For that purpose, one has to express that the elastic energy release rate is equal to Dupré reversible adhesion energy, according to Maugis and Barquins [24, 25].

This calculation is developed below, starting from the following definition of the elastic energy U_e, stored within the contact:

$$U_\mathrm{e} = \pi \int_0^\infty u(r)\sigma(r) r\mathrm{d}r. \tag{9}$$

Using the properties of Hankel transforms, this equation can be rewritten as follows in the transform space:

$$U_\mathrm{e} = \pi \int_0^\infty \xi \bar{u}(\xi)\bar{\sigma}(\xi)\mathrm{d}\xi. \tag{10}$$

From equations (3) and (4), it is possible to express the terms $\xi\bar{u}(\xi)$and $\bar{\sigma}(\xi)$ as cosine transforms of the auxiliary functions $g(s)$ and $\theta(s)$. If these cosine transforms are now substituted in equation (10), one gets the following expression for the elastic energy:

$$U_\mathrm{e} = 2\int_0^a \theta(s) g(s)\mathrm{d}s. \tag{11}$$

In order to determine the elastic energy release rate, the derivative of U_e at constant penetration, δ, must be evaluated. From equation (11), one gets

$$\frac{1}{2}\left.\frac{\partial U_\mathrm{e}}{\partial a}\right|_\delta = \theta(a) g(a) + \int_0^a \theta(s) \left.\frac{\partial g(s)}{\partial a}\right|_\delta \mathrm{d}s, \tag{12}$$

as, at a fixed penetration δ, $\theta(s)$ is independent on the radius, a.

Equation (5) therefore expresses the derivative $\partial g(s)/\partial a|_\delta$:

$$\left.\frac{\partial g(s)}{\partial a}\right|_\delta = -\frac{E_1^*}{2}\left[K(a, s) g(a) + \int_0^a K(\rho, s) \left.\frac{\partial g(\rho)}{\partial a}\right|_\delta \mathrm{d}\rho\right]. \tag{13}$$

If the expressions for $\theta(s)$ (equation (5)) and $\partial g(s)/\partial a|_\delta$ (equation (13)) are now replaced in equation (12) and if the symmetry of the kernel $K(\rho, s)$ is accounted for, the expression of the elastic energy release rate, $\mathcal{G}$, simplifies to

$$\mathcal{G} = \frac{1}{2\pi a}\left.\frac{\partial U_\mathrm{e}}{\partial a}\right|_\delta = \frac{2}{\pi a E_1^*} g^2(a). \tag{14}$$

At equilibrium, the use of the Griffith criterion, $\mathcal{G} = w$ [24, 25], yields

$$g(a) = \sqrt{\frac{\pi w a E_1^*}{2}}, \tag{15}$$

where w is the Dupré reversible thermodynamic work of adhesion.

From equation (14), it comes out that $g(a)$ is formally equivalent to the mode I stress intensity factor describing—within the framework of linear elastic fracture mechanics—the stress singularity induced by the adhesive forces at the periphery of the contact ($K_I = 2/\sqrt{\pi a}\, g(a)$ under plane strain conditions). It is worth noting that the obtained expression for K_I in a coated contact is strictly equivalent to that derived by Maugis [26] in the case JKR contacts on semi-infinite bodies. In other words, the stress singularity associated with the adhesion of the coated substrate appears to be only a function of the layer's modulus and not of the substrate's elastic properties. From a physical point of view, this result can be viewed as a consequence of the classical JKR assumption that

the adhesive forces vanish at the periphery of the contact. Then, the characteristic length associated with the effect of adhesion vanishes. As a consequence, the stress singularity associated with adhesion therefore becomes a purely local effect which only affects the layer. It is therefore identical to that derived for JKR contact by Maugis [26] from an extension of the Sneddon solution [27] for the frictionless axisymmetric Boussinesq problem.

According to (8) and (15), the solution for the adhesive contact of a layer on a substrate is, therefore, obtained from the following integral equation:

$$\sqrt{\frac{2aw}{E_1^*}} + \varphi(a) - \varphi(s) = \frac{2}{E_1^*} g(s) + \int_0^a \Delta K(\rho, s) g(\rho) \mathrm{d}\rho, \tag{16}$$

which can readily be solved numerically [17] in order to provide $g(s)$ values and the associated adhesive force

$$P = 4 \int_0^a g(s) \mathrm{d}s. \tag{17}$$

Once the function $g(s)$ is calculated, the penetration, δ, can be easily determined from equation (7).

In addition to the penetration and the load, this approach allows calculating the vertical displacement, $u(r)$, of the surface. From equation (4), $u(r)$ can be related as follows to $\theta(s)$ in the real space:

$$\theta(s) = \frac{\mathrm{d}}{\mathrm{d}s} \int_s^\infty \mathrm{d}r \frac{r u(r)}{\sqrt{s^2 - r^2}}, \tag{18}$$

which can be inverted as:

$$u(r) = \frac{\pi}{2} \int_0^r \mathrm{d}s \frac{\theta(s)}{\sqrt{r^2 - s^2}}, \tag{19}$$

where the function $\theta(s)$ can be determined for every value of the space coordinate s using the calculated values of $g(s)$ in equation (7). Putting $s = r \cos\alpha$, equation (14) turns into the following integral:

$$u(r) = \frac{\pi}{2} \int_0^{\pi/2} \mathrm{d}\alpha \theta(r \cos\alpha), \tag{20}$$

which can easily be evaluated numerically.

3.2. Implementation of the model

The details of the numerical procedure used to solve the adhesive contact problem are similar to that reported in [17], except for the value of $g(a)$ which was calculated from the layer's elastic properties and the adhesion energy using equation (12). As a verification, calculated adhesion curves relating the contact radius to the applied load were compared with the FE method model recently derived by Sridhar and Johnson [13–15]. According to Maugis [3], the load and the penetration were expressed in the following non-dimensional form:

$$\bar{P} = P/3\pi w R \qquad \bar{a} = a \left(\frac{4E_1^*}{9\pi w R^2} \right)^{1/3},$$

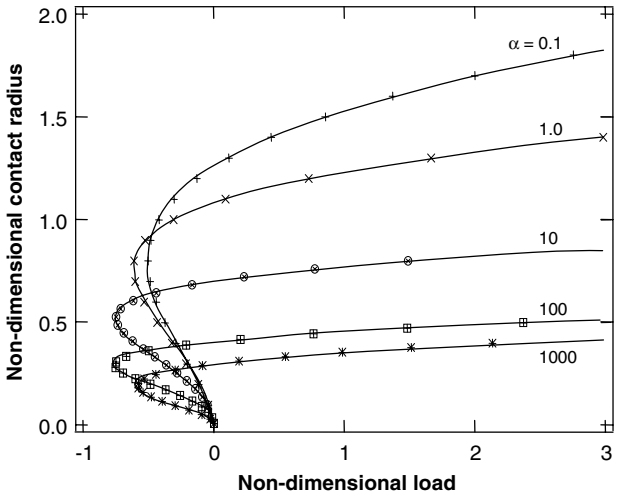

Figure 3. Theoretical variation of the non-dimensional contact radius with the non-dimensional load for a range of values of the adhesion parameter. The symbols correspond to data calculated using the semi-analytical model developed in this paper; the solids lines correspond to the F.E.M results obtained by Sridhar and Johnson using the same values of the adhesion parameter (data taken from [14]). ($\nu_0 = 0.2$, $\nu_1 = 0.4999$ and $E_0^*/E_1^* = 109.39$).

and the adhesion curves were calculated for various values of an adhesion parameter, α, defined as a non-dimensional measure of the work of adhesion:

$$\alpha = \left(\frac{2wR^2}{E_1^* t^3} \right)^{1/2}.$$

In figure 3, it can be seen that the present analytical calculations agree perfectly well with the previous FEM calculations by Sridhar and Johnson, which supports the validity of our model. It can also be pointed out that, for all the experimental situations addressed in this study, the theoretical calculations indicated that deformation of the substrate was negligible as compared with that of the layer.

4. Experimental results

4.1. Adhesion of bulk specimens

In a preliminary stage, the experimental procedure was validated using bulk acrylate specimens for which it was possible to apply the well established JKR theory. Once the contacts were cooled at room temperature, well distinguishable circular imprints were observed on the surface of the specimens (see insert in figure 4). The associated contact radii were measured for a set of glass lenses. Each of these lenses was characterized by a different radius of curvature which makes it impossible to reduce all the data in the usual $a^3(P)$ plot. However, the JKR theory indicates that all the experimental data should rescale onto a single relationship if a^3/R^2 is plotted as a function of P/R:

$$\frac{a^3}{R^2} = \frac{3}{4E_1^*} \left[\frac{P}{R} + 3\pi w + \sqrt{6\pi \frac{P}{R} + (3\pi w)^2} \right]. \tag{21}$$

The data reported in figure 4 show reasonable agreement with this assumption. From a least-square fit of the data points

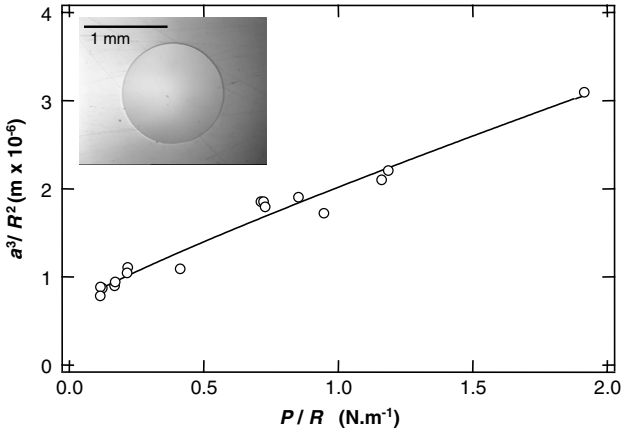

Figure 4. Reduced contact radius, a^3/R^2, versus reduced contact load, P/R, for bulk acrylate specimens. These experimental data were obtained using glass lens with radii of curvature, R, varying between 3.1 and 77.8 mm. The solid line corresponds to a theoretical calculation using the JKR theory (equation (21)) with $E_1^* = 0.9$ MPa and $w = 42$ mJ m^{-2}. Insert: optical microscope photograph of an adhesive imprint.

with equation (21), it was found that $E_1 = 0.67 \pm 0.05$ MPa (assuming $\nu_1 = 0.5$ as it is expected in the rubbery regime where the imprint is realized) and $w = 42 \pm 6$ mJ m^{-2}. The value of the elastic modulus, E_1, is in close agreement with independent measurements using dynamic mechanical thermal analysis [18]. No independent estimate was available for the adhesion energy of the glass/acrylate system under investigation, but the obtained value is in reasonable agreement with the published data for acrylate/glass systems [28].

It is worth noting that in the presented experiments, contact radius remains much less than the spherical lens radius. Then simple JKR theory for paraboloidal indenters should apply. No correction is expected as would be the case for larger contact sizes [5, 29]. For the experiments on thin layers described below, the soft elastic film lies on a rigid substrate which enhances considerably the overall contact stiffness. As a result, the measured contact radii are, again much less than the radii of the spheres.

4.2. Adhesion on film specimens

As a first analysis of the film systems, the radii of the adhesive contacts were measured from optical observations of the imprints. This set of data was used to estimate the value of the ratio w/E_1^* of the films. From a least square procedure using the adhesive contact model, an average value was obtained ($w/E_1^* = 38$ nm) which is consistent, with although slightly lower than, the bulk value ($w/E_1^* = 47$ nm).

A more refined analysis of the adhesive contacts was subsequently carried out using the recorded surface profile. Figure 5 shows two characteristic surface profiles of contact cross sections which were obtained under different geometrical confinements ($a/t = 4.5$ and $a/t = 9.1$). In both cases it can be seen that the junction of the elastic solid to the rigid spherical indenter is nearly vertical. Such an observation is consistent with the hypothesis of short range adhesive forces, which is embedded in the present adhesion model like in classical JKR theory.

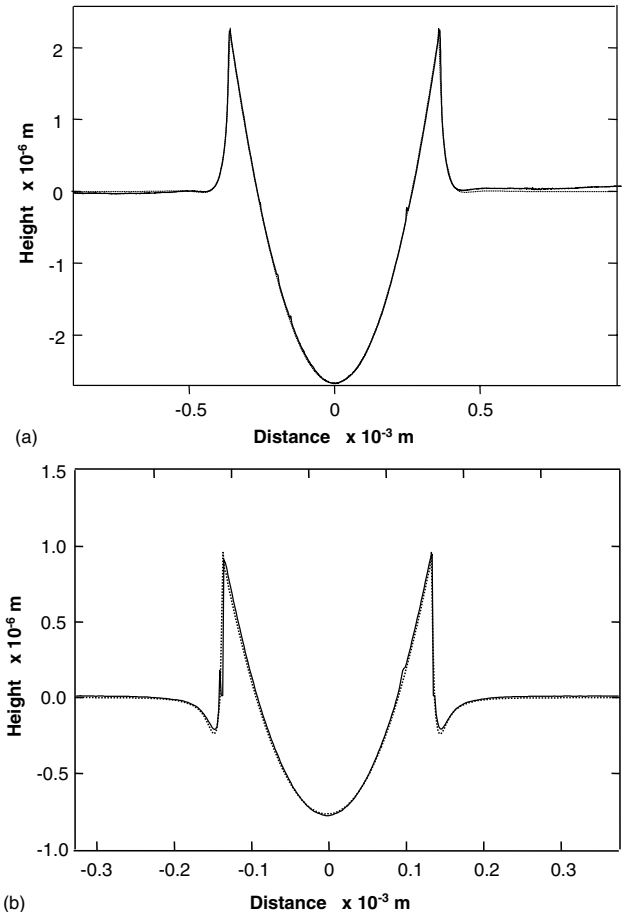

Figure 5. Theoretical (· · · · · ·) and experimental (——) surface profiles in the adhesive contact region for different confinement situations. (*a*) $t = 79\,\mu$m, $R = 12.9$ mm, $a/t = 4.6$ (*b*) $t = 15\,\mu$m, $R = 5.2$ mm, $a/t = 9.0$.

It was attempted to simulate these two experimental profiles using the adhesive contact model. The theoretical results reported in figure 5 show that an adjustment of the value of w/E_1^* close to the previously determined average value allows a very accurate simulation of the deformation within the contact zone. It can especially be seen that the adhesive model can simulate the progressive formation of a circular depression of the free surface close to the edge of the contact when the confinement of the contact is large.

4.3. Fingering instabilities in confined contacts geometries

Using glass lenses with larger radii of curvature, it was possible to enhance the level of geometrical confinement within the contact, i.e. the ratio a/t. Interestingly, it was observed that doing so resulted in the apparition of instabilities at the edge of the contact in the form of wavy undulations. An example is shown in figure 6 for an a/t ratio close to 40, where the wavelength of the instability is about seven times the film thickness. *In situ* observations of the contact zone during heating showed that these instabilities are generated during the formation of the adhesive contact.

Such observations are reminiscent of the meniscus instabilities which have been reported by Ghatak *et al* [30–32] in experiments with elastomeric films confined between a plane

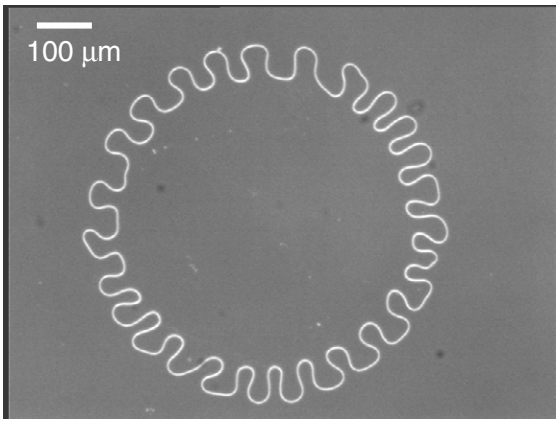

Figure 6. Generation of contact instabilities during the development of an adhesive contact under confined conditions. ($R = 51.8$ mm, $t = 15\,\mu$m). The contact confinement, a/t, is about 40.

rigid glass and a thin curved glass plate. In these studies, the authors found that the wavelength, λ, of the instabilities is proportional to the film thickness, t, with $\lambda/t \sim 4$, which is close to the value corresponding to figure 6. In their papers, Ghatak *et al* argued that the periodic deformation of the contact line can be explained by considering fluctuations of the surface forces, according to an argument initially introduced by Mönch *et al* [33].

A different analysis was developed by Schull and co-workers to analyse fingering instabilities which develop in confined elastic layers in tension within JKR contacts [34]. Extending to elastic solids the classic Saffman–Taylor analysis of flow instabilities in confined Newtonian fluids [35], these authors stated that fingering instabilities are driven by the release of lateral constraints within confined layers. Accordingly, the conditions for the occurrence of fingering were assumed to be related to the sign of the normal pressure gradient close to the periphery of the contacts. Some FE simulations for a flat punch adhesively bonded to a film under tension supported these hypotheses. These calculations showed that, for confined geometries, the normal pressure near the contact edge tends to increase in the direction of the interfacial motion, which is one of the requirements for Saffman–Taylor instabilities to occur. On the other hand, the pressure gradient was found to be negative toward the centre of the contact for low confinements, where no instabilities were observed.

A similar analysis for the JKR contacts under consideration is presented below from a calculation of the adhesive contact stresses within the layer. The latter was carried out using an approach close to that described by Li *et al* [19], which is detailed in appendix 1. As a first qualitative approach, the computations have been carried out for a zero normal force. In figure 7, the calculated normal stress distributions have been averaged through the thickness of the layer and reported for $a/t = 3$, $a/t = 12$. In passing, it can be noted that these averaged stresses does not show any singularity at the edge of the contact, as opposed to the surface stress distribution (figure 7). This is due to the fact that the stress singularity at the edge of the contact varies as $1/\sqrt{\rho}$, $\rho \to a$ [3], which integral over the thickness of the layer is finite. In figure 7, it can be seen that increased

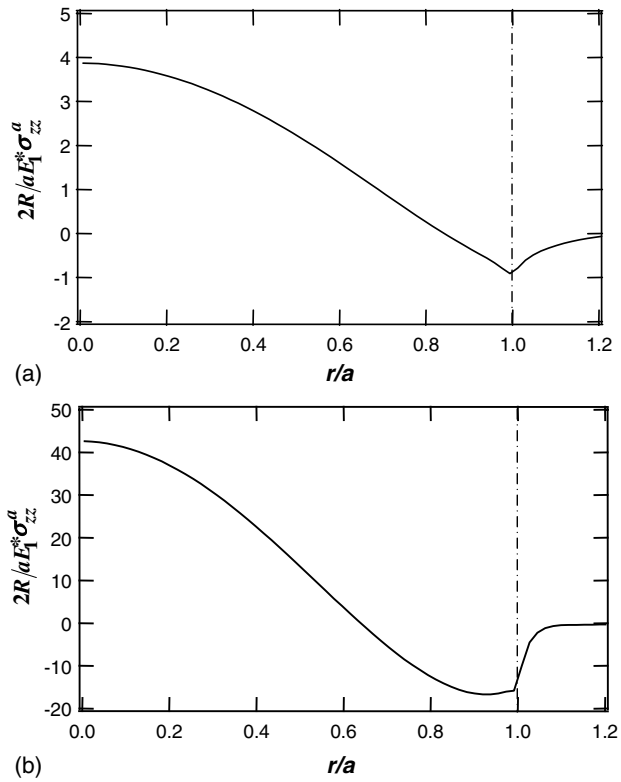

Figure 7. Calculated average normal stress, σ_{zz}^a, through the thickness of the layer in an adhesive contact with a sphere under zero normal load. (*a*) $a/t = 3$; (*b*) $a/t = 12$. ($E_0^*/E_1^* = 8 \times 10^4$, $w/E_1^* = 40$ nm, $\nu_0 = 0.2$, $\nu_1 = 0.5$).The calculation shows that confinement is associated with a change in the sign of the stress gradient close to the edge of the contact which is a criterion for the occurrence of Saffman–Taylor like instabilities.

levels of confinement result in a change in the sign of the normal stress gradient close to the edge of the contact. For a/t ratios greater than about 10, the normal stress near the contact edge tends to increase toward the centre of the contact, which fulfils the instability criterion proposed by Schull *et al* following the Saffman Taylor analysis. This stability analysis is consistent with the experimental observations which showed that instabilities appeared for a/t ratio greater than about 10. This analysis cannot, however, be extended to the regime where fingering instabilities are fully developed. Nevertheless, it seems realistic to assume that the lateral size of the fingers should be of the order of magnitude of the thickness of the layer as the instabilities are driven by the release of the lateral constraints associated with confinement. It is worth noting that in the previous experimental investigations, fingering instabilities were observed under the action of tensile forces. The present theoretical calculations and experimental observations show that such instabilities can also be generated under a vanishing or slightly compressive contact load.

5. Conclusion

In summary, a semi-analytical model for the adhesive contact of a rigid indenter on a coated substrate is presented. The resulting integral equation (equation (16)) can be rather easily numerically solved. This description is validated by

comparison with existing FEs calculations. An experimental validation is also proposed. By cooling down adhesive contact of spherical indenters on coated polymer substrates, it is shown that corresponding imprints can be frozen. They are shown to closely fit the shapes predicted by the model. It could, therefore, be envisaged to use these simple experiments to determine the adhesive and elastic properties of coated substrates. This would require, however, a careful analysis of the sensitivity of the contact behaviour to small fluctuations in the Poisson's ratio close to incompressibility. Previous theoretical calculations by Ganghoffer and Gent [11] have shown that this issue can be critical when the ratio of the contact radius to the film thickness exceeds a few unities.

When the radius of the spherical indenter is large, non-axisymmetric imprints are observed. The corresponding instability corresponds to the release of the elastic energy stored in the highly confined region of the film under the contact. These observations complement previous results reported by Schull *et al* [34] and Gathak *et al* [30–32] in the sense that they show that contact instabilities in confined geometries can, not only be observed under the action of tensile forces, but also for compressive or vanishing contact forces.

Thus, it seems important to extend the present study of the equilibrium adhesive contact on a coated substrate by an analysis of its stability. Moreover, as in the JKR model, a zero range adhesive force is included in the model. Situations which have been experimentally considered appear to correspond to this hypothesis. However, it can be anticipated that, either for thinner films or more rigid ones or smaller indenter radii such an assumption should fail, as it is similarly the case on semi-infinite substrates [26]. This limitation of the model should be further analysed.

Acknowledgments

Hélène Montes and Eric Gacoin are thanked for their help in the preparation and the characterization of the samples. Etienne Barthel is also thanked for many fruitful discussions. Many thanks are also due to E Lepleux (Scientec, France) for the measurements using the interferometric microscope.

Appendix 1

The calculation of the stresses within a layered adhesive contact was based on an approach similar to that developed by Li *et al* [19]. Taking into account the continuity of stresses and displacements at the film/substrate interface, analytical expressions were derived for the Hankel transforms of the stresses within the film. In this problem, the Hankel transforms of the surface stresses are taken as boundary conditions. In the case of frictionless adhesive contacts, this approach, therefore requires a knowledge of the Hankel transform of the normal surface pressure, which can be determined from a preliminary resolution of the adhesive contact problem using the procedure described in section 3.1.

When considering the direct inversion of the stress expressions in real space using a discrete Hankel transform algorithm, some numerical difficulties arise due to the existence of a stress singularity at the edge of the adhesive contact. This problem was circumvented by splitting the

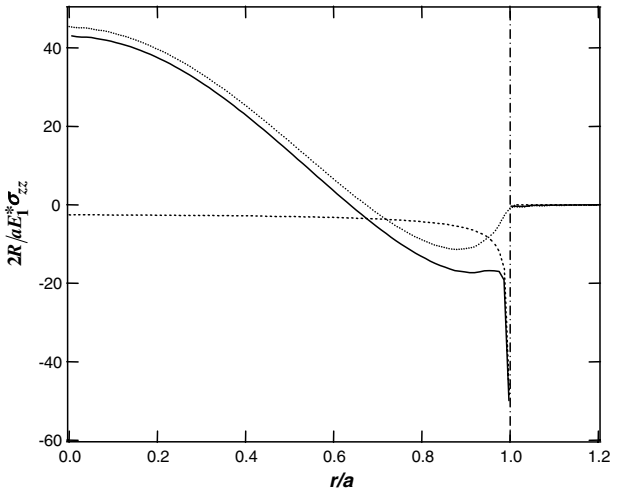

Figure 8. Calculation of the normal surface stress components corresponding to the terms $g(a)$ and $\Delta g(r)$ in equation (22). ($P = 0$, $E_0^*/E_1^* = 8 \times 10^4$, $w/E_1^* = 40\,\text{nm}$, $\nu_0 = 0.2$, $\nu_1 = 0.5$). The stress distribution corresponding to $g(a)$ (· · · · · ·) has been calculated analytically using the solution to the classical Boussinesq problem. The stress component associated with $\Delta g(r)$ (· · · · · ·) was inverted in real space using the discrete Hankel transform algorithm described in [36]. The normal surface stress (——) is obtained by summation of these two stress components.

function $g(r)$, i.e. the integral transform of the normal stress (cf equation (3)), into two separate components:

$$g(r) = g(a) + \Delta g(r), \tag{22}$$

where the constant term $g(a)$ corresponds to the classical Boussinesq problem of the frictionless indentation of a homogeneous semi-infinite body by a flat-ended cylindrical punch. This term, which contributes to the normal stress in an analytically known manner [27], incorporates the stress singularity associated with the adhesive contact. The additional term, $\Delta g(r)$, vanishes for $r = a$, which corresponds formally to a non adhesive contact situation. As a result, no singularity is obtained when the associated stress components are inverted in real space. We used here the discrete Hankel transform algorithm developed by Guizar-Sicairos *et al* [36].

This procedure is illustrated in figure 8, where the surface normal stress components corresponding to $g(a)$ and $\Delta g(r)$ have been reported separately. The surface normal stress is simply given by the addition of these two terms.

References

[1] Johnson K, Kendall K and Roberts A D 1971 Surface energy and the contact of elastic solids *Proc. R. Soc. Lond.* A **324** 301–13
[2] Barquins M 1992 Adherence, friction and wear of rubber-like materials *Wear* **158** 87–117
[3] Maugis D 1999 *Contact, Adhesion and Rupture of Elastic Solids* (Berlin: Springer)
[4] Deruelle M, Léger L and Tirrell M 1995 Adhesion at the solid-elastomer interface: influence of the interfacial chains *Macromolecules* **28** 7419–28
[5] Rimal D S, Quesnel D J and Bowen R C 2001 Particle adhesion to highly compliant substrates: anomalous power-law dependence of the contact radius on particle radius. *Langmuir* **17** 6946–52

[6] Basire C and Fretigny C 2001 Kinetics of adhesion on a viscoelastic sample by force microscopy. *Tribol. Lett.* **10** 189
[7] Wahl K J, Asif S A S, Greenwood J A and Johnson K L 2006 Oscillating adhesive contacts between micron-scale tips and compliant polymers *J. Colloid Interface Sci.* **296** 178–88
[8] Ebenstein D M and Wahl K J 2006 A comparison of JKR-based methods to analyze quasi-static and dynamic indentation force curves *J. Colloid. Interface Sci.* **298** 652–62
[9] Deruelle M, Hervet H, Jandeau G and Léger L 1998 Some remarks on JKR experiments *J. Adhes. Sci. Technol.* **12** 225–47
[10] Shull K R 2002 Contact mechanics and the adhesion of soft solids *Mat. Sci. Eng. Rep.* **36** 1–45
[11] Ganghoffer J F and Gent A N 1995 Adhesion of a rigid punch to a thin elastic layer *J. Adhes.* **48** 75–84
[12] Shull K R, Ahn D, Chen W L, Flanigan C M and Crosby A J 1998 Axisymetric adhesion tests of soft materials *Macromol. Chem. Phys.* **199** 489–511
[13] Johnson K L and Sridhar I 2001 Adhesion between a spherical indenter and an elastic solid with a compliant elastic coating *J. Appl. Phys. D: Appl. Phys.* **34** 683–9
[14] Sridhar I, Zheng Z W and Johnson K L 2004 A detailed analysis of adhesion mechanics between a compliant elastic coating and a spherical probe *J. Appl. Phys. D: Appl. Phys.* **37** 2886–95
[15] Sridhar I and Sivashanker S 2003 On the adhesion mechanics of multi-layer elastic systems *Surf. Coat. Technol.* **167** 181–7
[16] Sridhar I, Johnson K L and Fleck N A 1997 Adhesion mechanics of the surface force apparatus *J Appl Phys D* **30** 1710-9
[17] Perriot A and Barthel E 2004 Elastic contact to a coated half-space: Effective elastic modulus and real penetration *J. Mat. Res.* **19** 600-8
[18] Gacoin E, Chateauminois A and Fretigny C 2004 Measurements of the viscoelastic moduli of an acrylate polymer in bulk and film form using a contact method. *Polymer* **45** 3789–96
[19] Li J and Chou T-W 1997 Elastic field of a thin-film/substrate system under an axisymmetric loading *Int. J. Solids Struct.* **34** 4463–78
[20] Nogi T and Kato T 1997 Influence of a hard surface layer on the limit of elastic contacts. Part I: analysis using a real surface model *ASME J. Trib.* **119** 493–500
[21] Huguet A S and Barthel E 2000 Surface forces and the adhesive contact of axisymmetric elastic bodies *J. Adhes.* **74** 143–75
[22] Barthel E and Haiat G 2002 Approximate model for the adhesive contact of viscoelastic spheres *Langmuir* **18** 9362–70
[23] Barquins M and Maugis D 1982 Adhesive Contact of Axisymmetric Punches on an Elastic Half-Space-the Modified Hertz-Hubers Stress Tensor for Contacting Spheres *J. Mec. Theo. Appl.* **1** 331–57
[24] Maugis D 1985 Review on subcritical crack growth, surface energy, fracture toughness, stick-slip and embrittlement *J. Mater. Sci.* **20** 3041–73
[25] Maugis D and Barquins M 1978 Fracture mechanics and the adherence of viscoelastic bodies. *J. Appl. Phys. D: Appl. Phys.* **11** 1989–2023
[26] Maugis D 1992 Adhesion of spheres: the JKR-DMT transition using a Dugdale model *J. Colloid. Interface Sci.* **150** 243–69
[27] Sneddon I N 1965 The relation between load and penetration in the axisymmetric bousinesq problem for a punch of arbitrary profile *Int. J. Eng. Sci.* **3** 47–57
[28] Flanigan C M and Shull K R 1999 Adhesive and elastic properties of thin gel layers *Langmuir* **15** 4966–74
[29] Maugis D 1995 Extension of the Johnson-Kendall-Roberts theory of the elastic contact of spheres to large contact radii *Langmuir* **11** 679–82
[30] Ghatak A, Mahadevan L and Chaudhury M K 2005 Measuring the work of adhesion between a soft confined film and a flexible plate *Langmuir* **21** 1277–81
[31] Ghatak A and Chaudhury M K 2003 Adhesion-induced instability patterns in thin confined elastic film *Langmuir* **19** 2621–31
[32] Ghatak A, Chaudhury M J, Shenoy V and Sharma A 2000 Meniscus Instability in a thin elastic film *Phys. Rev. Lett.* **85** 4329–32
[33] Mönch W and Herminghaus S 2001 Elastic instabilities of rubber films between solid bodies *Europhys. Lett.* **53** 525-31
[34] Shull K R, Flanigan C M and Crosby A J 2000 Fingering instabilities of confined elastic layers in tension *Phys. Rev. Lett.* **84** 3057–60
[35] Saffman P G and Taylor G 1958 The penetration of a fluid into a porous medium or Hele-Shaw cell containing a more viscous liquid *Proc. R. Soc. Lond. Ser. A-Math. Phys. Sci.* **245** 312–29
[36] Guizar-Sicairos M and Gutiérrez-Vega J C 2004 Computation of quasi-discrete Hankel transforms of integer order for propagating optical wave fields. *J. Opt. Soc. Am.* A **21** 53–8